Desalination and Water Treatment
www.deswater.com

doi: 10.5004/dwt.2021.27326

228 (2021) 422–430
July

Treatment of Malachite green wastewater using walnut shell

Yinghua Song*, Shengming Chen, Hui Xu

Department of Chemistry and Chemical Engineering, Chongqing Technology and Business University, Chongqing 400067, China, Tel. +86-023-62769785; Fax: +86-023-62769785; emails: yhswjyhs@126.com (Y. Song), chensm5205@ctbu.edu.cn (S. Chen), xuhui@ctbu.edu.cn (H. Xu)

Received 20 October 2020; Accepted 12 April 2021

ABSTRACT

In this study, walnut shell (WS) was used to remove Malachite green (MG) from aqueous solutions through adsorption. Static experiments were performed to investigate the effects of different parameters including initial pH value, adsorbent dosage, contact time, and temperature on MG adsorption onto WS. It was found that both Langmuir and Freundlich isotherms could describe the equilibrium of MG onto WS. The maximum Langmuir adsorption capacity at 313 K was up to 1,477.33 mg g^{-1} WS. The removal efficiency was as high as 94.6% for 300 mg L^{-1} of MG concentration, pH = 6.0, a temperature of 303 K, and 6 g L^{-1} of WS dosage. Pseudo-second-order kinetics provided a better fit for the kinetic data of MG on WS. Intraparticle diffusion is an important rate-controlling step in the kinetic process, but it was not the only one. A method derived from the Langmuir equilibrium constant K_L was developed to determine the thermodynamic parameters, which proposes an endothermic spontaneous physisorption process. These findings imply that WS is a cost-effective, efficient, and very promising adsorbent for the treatment of MG wastewater.

Keywords: Walnut shell; Malachite green; Adsorption; Isotherm; Kinetics; Thermodynamics

1. Introduction

Large amounts of dye-based wastewaters are discharged from many industries, including textile, printing, leather, plastics, paper, food, and cosmetics, among others. Due to their highly toxic, teratogenic, and carcinogenic properties, these waters are associated with serious environmental effects and are hazardous to human beings [1]. Such dye-containing wastewaters must be treated before their discharge into water bodies. However, many dyes have complex aromatic ring structures that are difficult to be degraded. Therefore, the removal of such dyes has become an important factor in wastewater treatment. As an important cationic dye, Malachite green (MG) is widely applied in wool, leather, cotton, and silk products. In addition, it is used as a disinfectant and fungicide in fish farming, and animal husbandry. It has been reported that MG has a potential carcinogenic risk and may cause a variety of other diseases [2].

Among the various chemical and physical technologies to treat dye-based wastewater, adsorption is an inexpensive, fast, and universal method [3]. Currently, activated carbon is used to treat dye-containing wastewaters because of its high efficiency and simple operation. However, its operating costs are relatively expensive. Studies are evaluating cheaper and more effective alternatives for treating dyestuff wastewaters from different raw materials such as rice husks [4], banana peels [5], sugar beet bagasse [6], sawdust [7], tobacco residues [8], mango seeds [9], sago wastes [10], corn straws [11], peanut shells [12], and *Luffa aegyptica* peel [13], among others. These raw materials suggest a new and effective route for achieving low-cost and environmentally friendly goals in the industry. Furthermore, they show promise for use as adsorbents for dye removal from aqueous solutions.

* Corresponding author.

As an agricultural by-product, walnut shell (WS) is usually burned or directly discarded, producing waste gas and dust. Because of its good adsorption property, mechanical strength, and chemical stability, it has been successfully used to remove heavy metals (Cr(VI) [14], Cu(II) [15],) dyes (reactive brilliant red K-2BP [16], methylene blue [17]), and other organic substances (oil/water mixtures [18], dimethyl sulfide [19]) from waste-water. Activated carbon based on WS was synthesized for the removal of MG and a poor maximum Langmuir adsorption capacity of 11.76 mg g^{-1} adsorbent was obtained [20]. Studies have shown that several factors, including adsorbent dosage, pH, temperature, and contact time, affect the adsorption capacity. Therefore, this study aimed at evaluating the potential of WS to remove MG from aqueous solutions. Experiments were performed in a static system to evaluate the adsorption performance of WS from different aspects such as initial pH, adsorbent dosage, MG concentration, and temperature. A higher maximum Langmuir adsorption capacity of 1,477.33 mg g^{-1} WS at 313 K was obtained. A method derived from the Langmuir equilibrium constant, K_L, was used to predict the thermodynamic parameters. The MG adsorption mechanism of WS was deduced from the isotherms, kinetics, and thermodynamics results. This study provides a cheap, excellent, and promising biosorbent (WS) for MG removal in azo dye wastewater treatment.

2. Materials and methods

2.1. Adsorbent preparation

WS was purchased from a supermarket in Chongqing, China. First, WS was thoroughly cleaned using deionized water to remove dust and impurities and dried at 60°C in an oven. Then, it was ground into powder and sieved into different meshes before use.

2.2. Chemicals

0.5 g of MG was dissolved in 1 L of deionized water to prepare the stock solution, which was diluted to the desired concentrations (30–500 mg L^{-1}) to obtain test solutions. Initial pH of the solution was adjusted to a certain value using 1.0 mol L^{-1} of sodium hydroxide or hydrochloric acid solutions before the addition of WS.

2.3. Adsorption studies

A certain amount of WS (0.1–0.6 g) was added to 100 mL of MG solution (300 mg L^{-1}), after which the mixture was agitated at 150 rpm at a constant temperature (303–323 K). Samples were obtained at regular time intervals to spectrophotometrically determine residual MG concentrations at 617 nm. Experiments were repeated and mean values were taken for subsequent calculations.

For equilibrium studies, 0.02 g of WS was added to 100 mL of MG solution with concentrations ranging from 30 to 400 mg L^{-1}, then, mixtures were agitated at three different temperatures (298, 303, and 313 K) for 6 h. The kinetic and equilibrium data were non-linearly fitted using the Microcal OriginPro 8.5.1 software.

The adsorption capacity q (mg g^{-1}) and the percent removal efficiency %R was calculated as follows:

$$q = \frac{v\left(c_0 - c_t\right)}{m} \tag{1}$$

$$\%R = \frac{\left(c_0 - c_t\right)}{c_0} \times 100 \tag{2}$$

where c_0 and c_t are the initial concentration and the concentration at t moment (mg L^{-1}); v is the volume of MG solution used (L); and m is the mass of the dry WS used (g).

3. Results and discussion

3.1. Effect of Initial pH

Adsorption capacity increased sharply when initial pH of the solution rose from 2.0 to 6.0 while when pH was greater than 6.0, adsorption capacity decreased slowly (Fig. 1).

Under acidic conditions, excess H^+ ions in the solution will neutralize the negative charge on the WS surface, which inhibited the adsorption of cationic MG onto WS, resulting in lower MG removal. With increasing pH, protonation weakened and the available vacant sites on the WS surface became negatively charged, and the electrostatic attraction between positively charged cationic dye molecules and WS surface dominated [21]. However, when initial pH is greater than 6.0, the molecular structure of MG changes in an alkaline medium, and MG adsorption on WS exhibits a downward trend [22].

3.2. Effect of contact time and temperature

MG adsorption on WS was evaluated at an MG concentration of 300 mg L^{-1} and temperatures of 303, 313, and 323 K, respectively (Fig. 2). At the same concentration, the higher the temperature, the greater the equilibrium adsorption capacity, indicating that MG adsorption on WS was an endothermic process. Adsorption capacity of MG on WS increased from 88.4 mg g^{-1} at 303 K to 121.4 mg g^{-1} at 323 K.

As shown in Fig. 1, in the first 50 min MG removal was very fast, after which it gradually slowed down, and finally reached equilibrium in about 360 min. At the beginning, there were many vacant adsorption sites on WS and MG adsorption was very fast. As the vacant sites were gradually occupied, the adsorption process slowed down. As time went on, repulsive forces between bulk solution and MG molecules increased, inhibiting the occupancy of the remaining vacant sites. A similar finding was also reported regarding methylene blue adsorption onto eggshells [23].

3.3. Effect of the adsorbent dosage

As shown in Fig. 3, with increasing amounts of WS from 1 to 6 g L^{-1}, MG removal increased from 50.3% to 94.6% due to the increased surface area and the adsorption sites which enhanced MG adsorption [12]. However, when dosage increased to 6 g L^{-1}, the adsorption sites were close

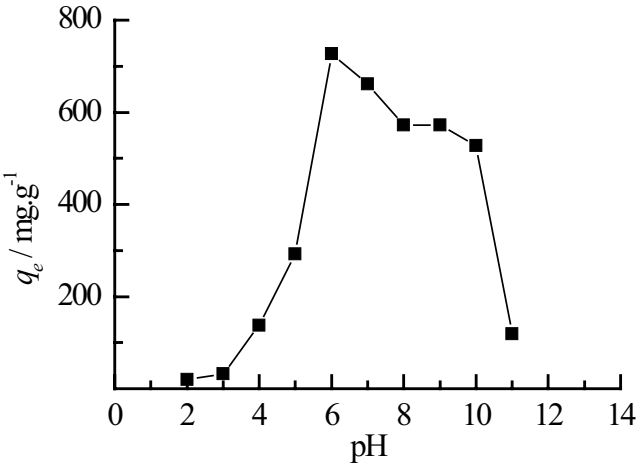

Fig. 1. Effect of pH (c_0 = 300 mg L^{-1}; T = 303 K; WS dosage = 0.2 g L^{-1}; contact time = 6 h; rpm = 150).

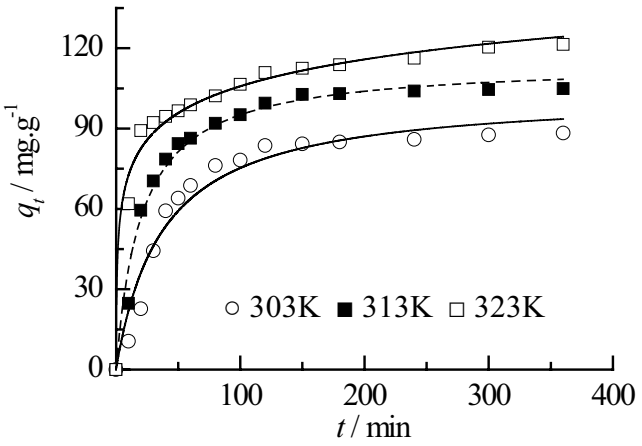

Fig. 2. Effect of contact time (c_0 = 300 mg L^{-1}; pH = 6.0 ± 0.1; WS dosage = 1 g L^{-1}; rpm = 150). The lines represented the best non-linear regression fits with pseudo-second-order kinetics.

to saturation, and the WS dosage had no longer significant impact on the removal efficiency of MG.

3.4. Adsorption isotherms and thermodynamic parameters

Three different adsorption isotherms, namely, the Langmuir, Freundlich, and Temkin were used to test the present system. Non-linear forms of adsorption isotherms were presented in the following forms.

$$q_e = \frac{q_{\max} K_L c_e}{1 + K_L c_e} \tag{3}$$

$$q_e = K_F c_e^{1/n} \tag{4}$$

$$q_e = \frac{RT}{b} \ln K_T + \frac{RT}{b} \ln c_e \tag{5}$$

where c_e (mg L^{-1}) is the equilibrium MG concentration, q_e (mg g^{-1}) and $q_{\max}$ (mg g^{-1}) the equilibrium and the maximum Langmuir adsorption capacity respectively, K_L, K_F, and K_T (L mg^{-1}) the Langmuir, the Freundlich, and the Temkin equilibrium constant, n (dimensionless) a constant related to the heterogeneity of the adsorbent, b (J mol^{-1}) the Temkin constant related to the heat of adsorption, R (8.314 J mol^{-1} K^{-1}) the ideal gas constant, and T (K) is the absolute temperature of the solution.

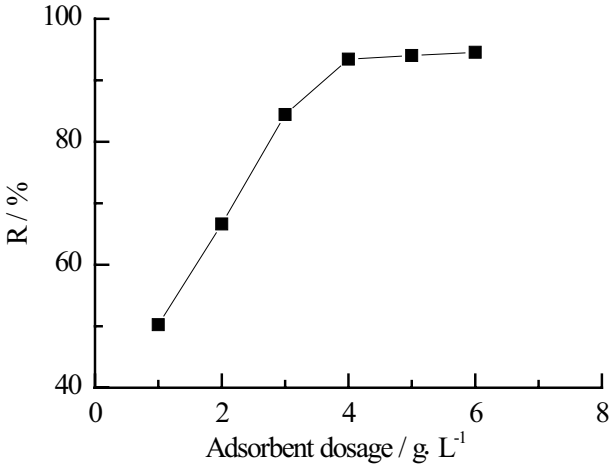

Fig. 3. Effect of absorbent dosage (c_0 = 300 mg L^{-1}; T = 303 K; pH = 6.0 ± 0.1; contact time = 6 h; rpm = 150).

As shown in Fig. 4, the adsorption capacity of MG on WS increased from 117.0 to 830.9 mg g^{-1} at 298 K, from 118.1 to 891.1 mg g^{-1} at 303 K, and from 118.6 to 995.9 mg g^{-1} at 313 K by increasing MG concentration. At the same temperature, the mass transfer driving force increased with the increase in initial MG concentration, and the interactions between MG and WS were enhanced, thereby increasing the loading capacity of WS.

An increase was also be observed in the equilibrium adsorption capacity when the temperature increased at the same concentration as shown in Fig. 4. The adsorption of MG on WS was enhanced by increasing temperature from 298 K to 313 K at different MG concentrations.

Three isotherms (the Langmuir, Freundlich, and Temkin models) were used to describe the equilibrium data. Correlation parameters are shown in Table 1. Based on R^2 comparisons, the adsorption equilibrium of MG onto WS can be both well described by the Langmuir and Freundlich equations. The Langmuir maximum adsorption capacity of 1,477.33 mg g^{-1} was obtained at 313 K and it increased with increasing temperature from 298 to 313 K, which indicated that MG adsorption on WS was an endothermic process. This phenomenon can be explained by the increased K_L and K_F values (Table 1) under higher temperatures due to the enhanced interaction forces between MG and WS [24]. All n values greater than 1 of the Freundlich equation indicated favorable adsorption [25]. According to Temkin isotherm, b values <20 J mol^{-1} are ascribed to the physisorption dominating chemisorption [26].

3.5. Thermodynamic parameters

The mechanism and rate-controlling step of the adsorption process can be elucidated by thermodynamic analysis

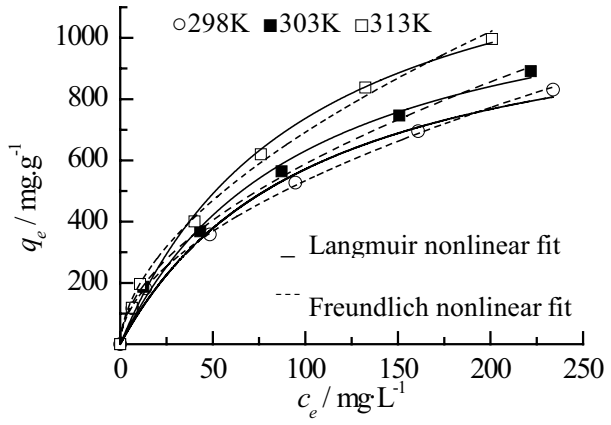

Fig. 4. Adsorption isotherms of MG onto WS (pH = 6.0 ± 0.1; adsorbent dosage = 0.2 g L^{-1}; contact time = 6 h; rpm = 150).

of the equilibrium data. Thermodynamic parameters, including free energy change, enthalpy, and entropy change, were calculated with the help of Eq. (6) [27].

$$\Delta G = \left(\Delta H - T\Delta S\right) = -RT\ln K_e \tag{6}$$

where K_e is the equilibrium constant.

The key factor for determining thermodynamic parameters using Eq. (6) is a correct K_e, which has been estimated using different methods. Various studies used the K_L of the Langmuir and K_F of the Freundlich isotherms instead of the K_e directly [28–30]. However, from Eq. (6), K_e is shown to be a dimensionless parameter. The Langmuir constant of K_L can be accepted as K_e when solute activity can be negligible only if the solution of the ionic solute is very dilute or the solute is a non-ionic one [31]. It has been suggested that K_L can be converted to a dimensionless K_e in Eq. (7) when K_L is expressed as L mg^{-1} [32] in an aqueous solution. The Freundlich equilibrium constant K_F can also be converted to a dimensionless K_e in Eq. (8) when K_F was expressed as (mg g^{-1})(L mg^{-1})$^{1/n}$ [33]. These calculation methods were recommended to be more accurate than the direct use of K_L and K_F [33].

$$K_{e1} = 10^6 K_L \tag{7}$$

$$K_{e2} = K_F \rho\left(\frac{10^6}{\rho}\right)\left(1 - 1/n\right) \tag{8}$$

where ρ is the density of pure water (~1.0 g mL^{-1}).

Recently, partition or distribution coefficient K_p, q_e/c_e or c_a/c_e (where c_a is the concentration of solute adsorbed onto the adsorbent), was often utilized directly as K_e [34,35], but the dimensionless one could be only obtained with Eq. (9) by plotting $\ln(c_a/c_e)$ vs. c_a and extrapolating to c_a = 0. If the plot is a straight line with a high correlative coefficient (R^2), K_p can be used as the correct value of K_e [32,33].

$$K_{e3} = K_p = \lim_{c_a \to 0} \frac{c_a}{c_e} \tag{9}$$

The Langmuir isotherm shows that the unit of K_L should be L mg^{-1} when the c_e is in mg L^{-1}. It can be changed into a dimensionless parameter by multiplying with a variable in mg L^{-1}, for example, 10^6 mg L^{-1}, the pure water concentration when the adsorbate was dissolved in water. From the q_e/c_e relationship, it should be reasonable that the unit of K_L be mg(adsorbate)/mg(adsorbent) over mg(adsorbate)/L (solution), that is, L(solution)/mg(adsorbent). The Langmuir equilibrium constant K_L can be converted into a dimensionless one by multiplying with mg (adsorbent)/L (solution) conducted in the system under investigation. Since 0.02 g of WS was added into 100 mL of solution in the present equilibrium study, we obtained K_{e4} by multiplying K_L with 200 mg L^{-1} (i.e., 0.02 g/100 mL) as Eq. (10).

$$K_{e4} = 200K_L \tag{10}$$

ΔG could also be calculated by the following equation since the present adsorption process could be well described by the Freundlich isotherm [36].

$$\Delta G = -nRT \tag{11}$$

where n is the Freundlich constant.

Different K_e values obtained from Eqs. (7)–(10) are shown in Table 2. The $\ln(c_a/c_e)$ vs. c_a plots are provided in Fig. 5. We considered the thermodynamic parameters calculated with K_{e2} to be accurate since the R^2 values were very high (all above 0.98). The obtained K_{e4} calculated by the newly established method in Table 2 was pretty close to K_{e3}, therefore, we believe the conversion of K_L by multiplying with mg(adsorbent)/L(solution) to obtain the dimensionless K_e is credible.

Thermodynamic parameters obtained using Eqs. (6)–(11) are shown in Table 3. Table 3 shows that the applied equilibrium constants exerted a significant impact on ΔG values. The ΔG values calculated by K_{e1} and K_{e2} are roughly the same, while ΔG calculated by K_{e3} and n are roughly

Table 1
Isotherms constants for the adsorption of MG on WS

T (K)	Langmuir constants			Freundlich constants			Temkin		
	q_{max} (mg g^{-1})	K_L (L mg^{-1})(10^{-3})	R^2	K_F	n	R^2	K_T (L mg^{-1})	b (J mol^{-1})	R^2
298	1,165.72	9.62	0.9870	45.62	1.87	0.9994	0.20	12.65	0.958
303	1,261.58	9.86	0.9905	48.69	1.85	0.9984	0.20	11.76	0.9608
313	1,477.33	10.01	0.9934	52.34	1.78	0.9956	0.20	10.50	0.9617

Table 2
K_e values of different methods

T (K)	K_L (L mg^{-1})10^{-3}	K_L (mg g^{-1})(L mg^{-1})$^{1/n}$	K_{e1} (10^6 K_L)	K_{e2} (K_Fρ(10^6/ρ)$^{(1-1/n)}$)	K_{e3} (K_p(R^2))	K_{e4} (200 K_L)
298	9.62	45.62	9,620	28,222	4.21(0.9811)	1.92
303	9.86	48.69	9,860	27,809	4.41(0.9896)	1.97
313	10.01	52.34	10,010	22,287	4.69(0.9929)	2.00

Table 3
Thermodynamic properties of the systems tested

T (K)	ΔG (kJ mol^{-1})						ΔH (R^2)(kJ mol^{-1})		ΔS (J mol^{-1} K^{-1})	
	K_L	K_{e1} (10^6 K_L)	K_{e2} (K_Fρ(10^6/ρ)$^{(1-1/n)}$)	K_{e3} (K_p(R^2))	K_{e4} (200 K_L)	n	K_{e3}	K_{e4}	K_{e3}	K_{e4}
298	11.51	–22.72	–25.39	–3.56(0.9747)	–1.62	–4.63				
303	11.64	–23.17	–25.78	–3.74(0.9861)	–1.71	–4.66	5.47(0.9968)	1.93(0.9714)	30.3	11.9
313	11.98	–23.97	–26.05	–4.02(0.9905)	–1.81	–4.63				

the same, with the former being about 6 times as much as the latter. ΔG calculated by K_{e4} (200 K_L) is much closer to that calculated by K_{e3} (K_p). Negative ΔG values that were derived from the K_{e1}, K_{e2}, K_{e3}, K_{e4} (dimensionless) constants, and n revealed that the adsorption process was spontaneous [37], while the positive ΔG value calculated by K_L (L mg^{-1}) directly provided an opposite sign. Therefore, a diverse and contradictory result was deduced regarding the spontaneity of the adsorption process. However, since WS exhibited excellent MG adsorption capacities, it can be concluded that this adsorption process was spontaneous. Furthermore, ΔG values decreased from –1.62 to –1.81 kJ mol^{-1} with increasing temperature, which suggested that adsorption was more spontaneous at higher temperatures [38].

The positive ΔH values proved that this adsorption process was endothermic, consistent with the experimental data. Regarding the ΔH absolute value, it is less than 40 kJ mol^{-1}, suggesting a typical physisorption process [39]. The calculated positive values for ΔS reflected a MG-WS affinity and increased randomness on the WS surface. Similar results were reported regarding MG adsorption by activated carbons [39] and biosorption of Erythrosine B onto Raphiahookeri seeds [40].

Different methods were used to calculate the thermodynamic parameters. However, an appropriate method has not been established. In this study, we developed a new method derived from K_L to calculate thermodynamic parameters, and the obtained ΔG was pretty close to that calculated by K_p.

3.6. Adsorption kinetics

Several consecutive steps are generally involved in the adsorption process and kinetic studies may help us to establish which one is the rate-limiting step. For this purpose, experimental data were compared with those predicted by the pseudo-first-order [41], pseudo-second-order models [42], the intraparticle diffusion kinetics [43], the Elovich models [44], and the Wünwald–Wagner intraparticle diffusion model [45]. The five kinetic models are obtained using Eqs. (12)–(16).

$$q_t = q_e\left(1 - e^{-k_1 t}\right) \tag{12}$$

$$q_t = \frac{k_2 q_e^2 t}{1 + k_2 q_e t} \tag{13}$$

$$q_t = \frac{1}{\beta}\ln\left(\alpha\beta\right) + \frac{1}{\beta}\ln\left(t\right) \tag{14}$$

$$q_t = K_p t^{1/2} + C \tag{15}$$

$$\log\left(1 - \frac{q_t}{q_e}\right) = \log\left(\frac{6}{\pi^2}\right) - \frac{4\pi^2 D}{2.303 d^2} t \tag{16}$$

where k_1 (min^{-1}) is the rate constant for the first-order, k_2 (g mg^{-1} min^{-1}) the rate constant for the second-order, K_p (mg min$^{-1/2}$ g^{-1}) the rate constant for the intraparticle diffusion models, C (mg g^{-1}) a parameter related to the boundary layer, α (mg g^{-1} min^{-1}) the initial desorption rate, β (g mg^{-1}) the Elovich desorption constant, d (cm) the mean particle diameter, and D (cm^2 s^{-1}) is the intraparticle diffusion coefficient.

The non-linear fit of the pseudo-second-order model is shown in Fig. 2. Parameters of these five models are shown in Table 4.

Considering the low R^2 values, and the large difference between equilibrium adsorption capacity calculated by the model and experimental data, the pseudo-first-order kinetic model could not give an ideal fit. At all three temperatures, high correlative coefficients (>0.95) of the pseudo-second-order kinetics were obtained. Besides, calculated q_e values were much close to the experimental data with the pseudo-second-order kinetics. These findings revealed that MG kinetics on WS could be well represented by the pseudo-second-order model. This is further supported by the finding of Ojediran et al. [46] where functionalized *Zea mays* cob was used for MG adsorption. Given that all R^2 values were less than 0.95, the Elovich model was also not suitable for describing the MG adsorption onto WS.

Due to the long time to reach equilibrium in our experiment, the effects of intraparticle diffusion should be considered. To elucidate the problem, the intraparticle diffusion model was used to describe the kinetic data (Fig. 6). The time dependence of q_t in Fig. 6 could be presented in three straight lines with correlation coefficients all greater than 0.90. Multi-linear characteristics indicated that intraparticle diffusion was dominant in MG adsorption [47,48]. Estimated rate constants of intraparticle diffusion revealed that $K_{p1} > K_{p2} > K_{p3}$, which is attributed to a change in diffusion rate during the multi-step adsorption process, wherein the first step, MG molecules rapidly diffused from the bulk solution to the WS surface, then, the MG molecules entered the WS micropores in the second step, the

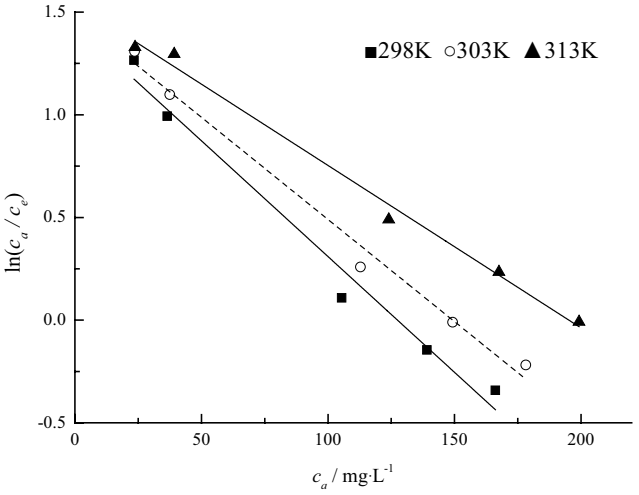

Fig. 5. The plot of $\ln(c_a/c_e)$ vs. c_a (pH = 6.0 ± 0.1; adsorbent dosage = 0.2 g L^{-1}; contact time = 6 h; rpm = 150).

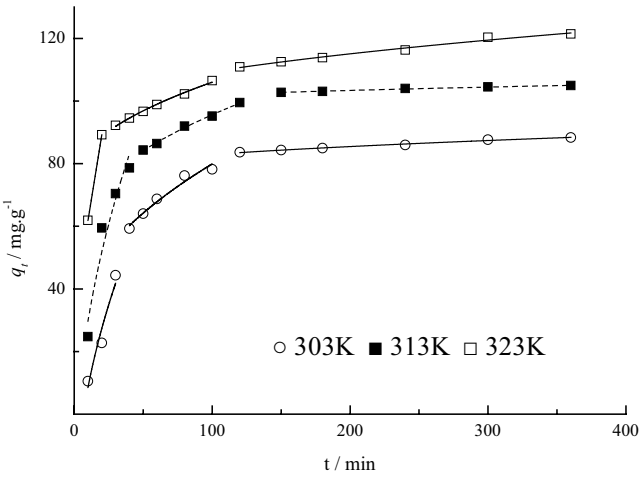

Fig. 6. Intraparticle diffusion plot for MG adsorption on WS.

Table 4
Statistical results of the application of the kinetic models

Model			Temperature (K)		
			303	313	323
First-order kinetic	k_1	Rate constant, min^{-1}	13.53	17.05	19.98
	$q_{e,cal}$	Equilibrium capacity, mg g^{-1}	67.07	86.42	102.68
	R^2	Correlation coefficient	0.2913	0.4743	0.7342
Second-order kinetic	k_2 (10^{-4})	Rate constant, g mg^{-1} min^{-1}	2.61	4.26	9.00
	$q_{e,cal}$	Equilibrium capacity, mg g^{-1}	103.21	114.56	119.52
	R^2	Correlation coefficient	0.9548	0.9822	0.9851
Elovich	α	Rate constant, mg g^{-1} min^{-1}	5.63	18.64	218.16
	β	Elovich constant, g mg^{-1}	0.045	0.050	0.069
	R^2	Correlation coefficient	0.9201	0.9328	0.9436
Intraparticle diffusion	K_{p1}	Rate constant, mg $min^{-1/2}$ g^{-1}	14.35	16.86	3.73
	C_1		–36.83	–23.60	34.56
	R_1^2	Correlation coefficient	0.9005	0.9060	1
	K_{p2}	Rate constant, mg $min^{-1/2}$ g^{-1}	5.36	3.90	3.12
	C_2		26.34	56.57	74.81
	R_2^2	Correlation coefficient	0.9784	0.9943	0.9939
	K_{p3}	Rate constant, mg $min^{-1/2}$ g^{-1}	0.61	0.34	1.38
	C_3		76.87	98.62	95.58
	R_3^2	Correlation coefficient	0.9877	0.9839	0.9810
Wünwald–Wagner intraparticle diffusion	D (10^{-9})	Effective diffusion coefficient, cm^2 s^{-1}	1.37	1.07	1.32
		Intercept	–0.30	–0.46	–0.43
	R^2	Correlation coefficient	0.8803	0.9676	0.8626
$q_{e,exp}$		Experimental data of the equilibrium capacity, mg g^{-1}	90.17	107.07	123.91

Table 5
Comparison of adsorption capacities of various adsorbents for MG

Adsorbent	Langmuir q_{max} (mg g^{-1})	T (°C)	References
WS	1,477.33	40	Present work
Activated carbon	91.24	45	[39]
Functionalized *Zea mays* cob	64.52	25	[46]
Reduced graphene oxide (rGO)	588.23	25	[47]
Reduced sulfonated graphene oxide (rGO–SO_3H)	1,111.11	25	[47]
Hematite iron oxide nanoparticles (α-Fe_2O_3)	952.98	50	[48]
Mesoporous magnetic biochar composite	515.77	25	[49]
Ackee apple seed–bentonite composite	706.72	25	[52]
Chitosan-deep eutectic solvents beads	17.86	–	[53]
Activated biochar derived from *Opuntia ficus-indica*	1,341	30	[54]
Mesoporous chitosan–zinc oxide composite	11	25	[55]
Brewers' spent	2.55	–	[56]
Magnetic graphene oxide	560.58	35	[57]

diffusion resistance increased, which led to decreased K_{p2}. Finally, in the third step, MG molecules tardily diffused into the WS internal micropores until an equilibrium was reached [49,50]. However, the multi-linear plots did not pass through the origin of coordinates, which indicated that film diffusion and intraparticle diffusion occurred simultaneously [46].

Magnitudes of the internal diffusion coefficient of the Wünwald–Wagner intraparticle diffusion model were 10^{-9}, which suggested that intraparticle diffusion was involved in MG adsorption onto WS, but was not the unique rate-limiting step [51].

3.7. Comparison of the q_{max} of various adsorbents

The Langmuir maximum MG adsorption capacities of some of the previously reported adsorbents in literature were compared to WS in Table 5. q_{max} of WS for MG was 1,477 mg g^{-1} at 313 K in this study which was significantly higher than most of the reported adsorbents. Moreover, most of the other adsorbents were derived from chemically modified natural materials, which increased adsorbent costs. Table 5 shows that WS is an effective low-cost adsorbent for the removal of MG dyes from aqueous solutions.

4. Conclusions

We investigate the efficiency of MG adsorption onto WS. Moreover, the influence of various parameters including particle size, pH value, temperature, and initial MG concentration on adsorption was evaluated. Both Langmuir and Freundlich isotherms ideally described the adsorption equilibrium. The maximum Langmuir adsorption capacity reached 1,477.33 mg g^{-1} WS at 313 K, while removal efficiency reached 94.6% for 300 mg L^{-1} of MG concentration, pH = 6.0 at a temperature of 303 K, and 6 g L^{-1} of WS dosage. Thermodynamic constants of the process were determined using a method derived from the Langmuir equilibrium constant K_L. Negative values of ΔG and the positive values of ΔH indicated the spontaneous endothermic nature of the process. The positive values of ΔS exhibited an increasing disorder at the solid-solution interface. The pseudo-second-order model provided a better fit of the kinetic data while the intraparticle diffusion model gave multi-linear plots, which indicated that the intraparticle diffusion was involved during this process. The WS can be used as a low-cost and efficient adsorbent for MG removal.

Acknowledgment

The work was supported by the Project Foundation of Chongqing Municipal Education Committee (KJ1600619).

References

[1] F. Marrakchi, B.H. Hameed, E.H. Hummadi, Mesoporous biohybrid epichlorohydrin crosslinked chitosan/carbon–clay adsorbent for effective cationic and anionic dyes adsorption, Int. J. Biol. Macromol., 163 (2020) 1079–1086.
[2] F. Jiang, D.M. Dinh, Y.-L. Hsieh, Adsorption and desorption of cationic malachite green dye on cellulose nanofibril aerogels, Carbohydr. Polym., 173 (2017) 286–294.
[3] N.A.H.M. Zaidi, L.B.L. Lim, A. Usman, Enhancing adsorption of malachite green dye using base-modified *Artocarpus odoratissimus* leaves as adsorbents, Environ. Technol. Innovation, 13 (2019) 211–223.
[4] M. Mobarak, E.A. Mohamed, A.Q. Selim, M.F. Eissa, M.K. Seliem, Experimental results and theoretical statistical modeling of malachite green adsorption onto MCM–41 silica/rice husk composite modified by beta radiation, J. Mol. Liq., 273 (2019) 68–82.
[5] A. Stavrinou, C.A. Aggelopoulos, C.D. Tsakiroglou, Exploring the adsorption mechanisms of cationic and anionic dyes onto agricultural waste peels of banana, cucumber and potato: adsorption kinetics and equilibrium isotherms as a tool, J. Environ. Chem. Eng., 6 (2018) 6958–6970.
[6] F. Ghorbani, S. Kamari, S. Zamani, S. Akbari, M. Salehi, Optimization and modeling of aqueous Cr(VI) adsorption onto activated carbon prepared from sugar beet bagasse agricultural waste by application of response surface methodology, Surf. Interfaces, 18 (2020) 100444, doi: 10.1016/j.surfin.2020.100444.
[7] L. Sun, D.M. Chen, S.G. Wan, Z.B. Yu, Performance, kinetics, and equilibrium of methylene blue adsorption on biochar derived from eucalyptus saw dust modified with citric, tartaric, and acetic acids, Bioresour. Technol., 198 (2015) 300–308.

[8] S. Archin, S.H. Sharifi, G. Asadpour, Optimization and modeling of simultaneous ultrasound-assisted adsorption of binary dyes using activated carbon from tobacco residues: response surface methodology, J. Cleaner Prod., 239 (2019) 118136, doi: 10.1016/j.jclepro.2019.118136.
[9] K. Shahul Hameed, P. Muthirulan, M. Meenakshi Sundaram, Adsorption of chromotrope dye onto activated carbons obtained from the seeds of various plants: equilibrium and kinetics studies, Arabian J. Chem., 10 (2017) S2225–2233.
[10] M. Karthika, M. Vasuki, Adsorption of Alizarine Red-S dye from aqueous solution by sago waste: resolution of isotherm, kinetics and thermodynamics, Mater. Today: Proc., 14 (2019) 358–367.
[11] S. Chen, G. Chen, H. Chen, Y. Sun, X.X. Yu, Y.J. Su, S.S. Tang, Preparation of porous carbon-based material from corn straw via mixed alkali and its application for removal of dye, Colloids Surf., A, 568 (2019) 173–183.
[12] D. Garg, C.B. Majumder, S. Kumar, B. Sarkar, Removal of direct blue-86 dye from aqueous solution using alginate encapsulated activated carbon (PnsAC-alginate) prepared from waste peanut shell, J. Environ. Chem. Eng., 7 (2019) 103365, doi: 10.1016/j.jece.2019.103365.
[13] F. Mashkoor, A. Nasar, Preparation, characterization and adsorption studies of the chemically modified *Luffa aegyptica* peel as a potential adsorbent for the removal of malachite green from aqueous solution, J. Mol. Liq., 274 (2019) 315–327.
[14] M. Banerjee, R.K. Basu, S.K. Das, Cr(VI) adsorption by a green adsorbent walnut shell: adsorption studies, regeneration studies, scale-up design and economic feasibility, Process Saf. Environ. Prot., 116 (2018) 693–702.
[15] R.M. Ali, H.A. Hamad, M.M. Hussein, G.F. Malash, Potential of using green adsorbent of heavy metal removal from aqueous solutions: adsorption kinetics, isotherm, thermodynamic, mechanism and economic analysis, Ecol. Eng., 91 (2016) 317–332.
[16] J.-S. Cao, J.-X. Lin, F. Fang, M.-T. Zhang, Z.-R. Hu, A new absorbent by modifying walnut shell for the removal of anionic dye: kinetic and thermodynamic studies, Bioresour. Technol., 163 (2014) 199–205.
[17] Y. Miyah, A. Lahrichi, M. Idrissi, A. Khalil, F. Zerrouq, Adsorption of methylene blue dye from aqueous solutions onto walnut shells powder: equilibrium and kinetic studies, Surf. Interfaces, 11 (2018) 74–81.
[18] J. Li, Z.H. Zhao, D.M. Li, X.H. Tang, H. Feng, W. Qi, Q. Wang, Multifunctional walnut shell layer used for oil/water mixtures separation and dyes adsorption, Appl. Surf. Sci., 419 (2017) 869–874.
[19] H. Jalilvand, F. Feyzi, M.R. Dehghani, Adsorption of dimethyl sulfide from model fuel on raw and modified activated carbon from walnut and pistachio shell origins: kinetic and thermodynamic study, Colloids Surf., A, 593 (2020) 124620, doi: 10.1016/j.colsurfa.2020.124620.
[20] S. Hajialigol, S. Masoum, Optimization of biosorption potential of nano biomass derived from walnut shell for the removal of Malachite Green form liquids solution: experimental design approaches, J. Mol. Liq., 286 (2019) 110904, doi: 10.1016/j.molliq.2019.110904.
[21] A.A. Adenuga, O.D. Amos, J.A.O. Oyekunle, E.H. Umukoro, Adsorption performance and mechanism of a low-cost biosorbent from spent seedcake of *Calophyllum inophyllum* in simultaneous cleanup of potentially toxic metals from industrial wastewater, J. Environ. Chem. Eng., 7 (2019) 103317, doi: 10.1016/j.jece.2019.103317.
[22] X. Wang, C. Jiang, B. Hou, Y. Wang, C. Hao, J. Wu, Carbon composite lignin-based adsorbents for the adsorption of dyes, Chemosphere, 206 (2018) 587–596.
[23] M.A. Abdel-Khalek, M.K.A. Rahman, A.A. Francis, Exploring the adsorption behavior of cationic and anionic dyes on industrial waste shells of egg, J. Environ. Chem. Eng., 5 (2017) 319–327.
[24] J. Dong, Y. Du, R. Duyu, Y. Shang, S. Zhang, R. Han, Adsorption of copper ion from solution by polyethylenimine modified wheat straw, Bioresour. Technol. Rep., 6 (2019) 96–102.
[25] G.K. Cheruiyot, W.C. Wanyonyi, J.J. Kiplimo, E.N. Maina, Adsorption of toxic crystal violet dye using coffe husks: equilibrium, kinetics and thermodynamics study, Sci. Afr., 5 (2019) e00116.
[26] Z. Zaheer, W.A. Bawazir, S.M. Al-Bukhari, A.S. Basaleh, Adsorption, equilibrium isotherm, and thermodynamic studies to the removal of acid orange 7, Mater. Chem. Phys., 232 (2019) 109–120.
[27] N. Fallah, M. Taghizadeh, S. Hassanpour, Selective adsorption of Mo(VI) ions from aqueous solution using a surface-grafted Mo(VI) ion imprinted polymer, Polymer, 144 (2018) 80–91.
[28] A. Saraeian, A. Hadi, F. Raji, A. Ghassemi, M. Johnson, Cadmium removal from aqueous solution by low-cost native and surface modified *Sorghum x drummondii* (Sudangrass), J. Environ. Chem. Eng., 6 (2018) 3322–3331.
[29] E. Nishikawa, M.G.C. da Silva, M.G.A. Vieira, Cadmium biosorption by alginate extraction waste and process overview in Life Cycle Assessment context, J. Cleaner Prod., 178 (2018) 166–175.
[30] K.-Y. Andrew Lin, Y.-T. Hsie, Copper-based metal organic framework (MOF), HKUST-1, as an efficient adsorbent to remove *p*-nitrophenol from water, J. Taiwan Inst. Chem. Eng., 50 (2015) 223–228.
[31] M.C. Stanciu, M. Nichifo, Influence of dextran hydrogel characteristics on adsorption capacity for anionic dyes, Carbohydr. Polym., 199 (2018) 75–83.
[32] H.N. Tran, S. You, H. Chao, Thermodynamic parameters of cadmium adsorption onto orange peel calculated from various methods: a comparison study, J. Environ. Chem. Eng., 4 (2016) 2671–2682.
[33] H.N. Tran, S.-J. You, A. Hosseini-Bandegharaei, H.-P. Chao, A mistake and inconsistencies regarding adsorption of contaminants from aqueous solutions: a critical review, Water Res., 120 (2017) 88–116.
[34] A. Kumar, H.M. Jena, Adsorption of Cr(VI) from aqueous phase by high surface area activated carbon prepared by chemical activation with $ZnCl_2$, Process Saf. Environ. Prot., 109 (2017) 63–71.
[35] D. Singh, S.K. Singh, N. Atar, V. Krishna, Amino acid functionalized magnetic nanoparticles for removal of Ni(II) from aqueous solution, J. Taiwan Inst. Chem. Eng., 67 (2016) 148–160.
[36] Y. Song, R. Peng, S. Chen, Y. Xiong, Adsorption of crystal violet onto epichlorohydrin modified corncob, Desal. Water Treat., 154 (2019) 376–384.
[37] R. Khamirchi, A. Hosseini-Bandegharaei, A. Alahabadi, S. Sivamani, A. Rahmani-Sani, T. Shahryari, I. Anastopoulos, M. Miri, H.N. Tran, Adsorption property of Br-PADAP-impregnated multiwall carbon nanotubes towards uranium and its performance in the selective separation and determination of uranium in different environmental samples, Ecotoxicol. Environ. Saf., 150 (2018) 136–143.
[38] S. Biswas, S.S. Mohapatra, U. Kumari, B.C. Meikap, T.K. Sen, Batch and continuous closed circuit semi-fluidized bed operation: removal of MB dye using sugarcane bagasse biochar and alginate composite adsorbents, J. Environ. Chem. Eng., 8 (2020) 103637, doi: 10.1016/j.jece.2019.103637.
[39] W. Qu, T. Yuan, G. Yin, S. Xu, Q. Zhang, H. Su, Effect of properties of activated carbon on malachite green adsorption, Fuel, 249 (2019) 45–53.
[40] C.C. Okoye, O.D. Onukwuli, C.F. Okey-Onyesolu, Utilization of salt activated *Raphia hookeri* seeds as biosorbent for Erythrosine B dye removal: kinetics and thermodynamics studies, J. King Saud Univ. Sci., 31 (2019) 849–858.
[41] S. Lagergren, About the theory of so-called adsorption of soluble substances, Kungl. Svenska Vetenskapsakademiens Handlingar, 24 (1898) 1–39.
[42] Y.S. Ho, G. McKay, Pseudo-second order model for sorption processes, Process Biochem., 34 (1999) 451–465.
[43] W.J. Weber, J.C. Morriss, Kinetics of adsorption on carbon from solution, J. Sanit. Eng. Div., 89 (1963) 31–60.
[44] R. Nodehi, H. Shayesteh, A.R. Kelishami, Enhanced adsorption of Congo red using cationic surfactant functionalized zeolite

particles, Microchem. J., 153 (2020) 104281, doi: 10.1016/j.microc.2019.104281.
[45] Y. Song, H. Xu, J. Ren, Adsorption study for removal of sunset yellow by ethylenediamine modified peanut husk, Desal. Water Treat., 57 (2016) 17585–17592.
[46] J.O. Ojediran, A.O. Dada, S.O. Aniyi, R.O. David, Functionalized *Zea mays* Cob (FZMC) as low-cost agrowaste for effective adsorption of malachite green dyes data set, Chem. Data Collect., 30 (2020) 100563, doi: 10.1016/j.cdc.2020.100563.
[47] E.G. Söğüt, Y. Karataş, M. Gülcan, N.Ç. Kılıç, Enhancement of adsorption capacity of reduced graphene oxide by sulfonic acid functionalization: Malachite green and Zn(II) uptake, Mater. Chem. Phys., 256 (2020) 123662, doi: 10.1016/j.matchemphys.2020.123662.
[48] A. Dehbi, Y. Dehmani, H. Omari, A. Lammini, K. Elazhari, A. Abdallaoui, Hematite iron oxide nanoparticles (α-Fe_2O_3): synthesis and modelling adsorption of malachite green, J. Environ. Chem. Eng., 8 (2020) 103394, doi: 10.1016/j.jece.2019.103394.
[49] A.S. Eltaweil, H.A. Mohamed, E.M.A. El-Monaem, G.M. El-Subruit, Mesoporous magnetic biochar composite for enhanced adsorption of malachite green dye: characterization, adsorption kinetics, thermodynamics and isotherms, Adv. Powder Technol., 31 (2020) 1253–1263.
[50] A. Moosavi, A.A. Amooey, A.A. Mir, M.H. Marzbali, Extraordinary adsorption of acidic fuchsine and malachite green onto cheap nano-adsorbent derived from eggshell, Chin. J. Chem. Eng., 28 (2020) 1591–1602.
[51] M. Liu, X. Li, Y. Du, R. Han, Adsorption of methyl blue from solution using walnut shell and reuse in a secondary adsorption for Congo red, Bioresour. Technol. Rep., 5 (2019) 238–242.
[52] M.A. Adebayo, J.I. Adebomi, T.O. Abe, F.I. Areo, Removal of aqueous Congo red and malachite green using ackee apple seed–bentonite composite, Colloid Interface Sci. Commun., 38 (2020) 100311, doi: 10.1016/j.colcom.2020.100311.
[53] A.C. Sadiq, N.Y. Rahim, F.B.M. Suah, Adsorption and desorption of malachite green by using chitosan-deep eutectic solvents beads, Int. J. Biol. Macromol., 164 (2020) 3965–3973.
[54] M. Choudhary, R. Kumar, S. Neogi, Activated biochar derived from *Opuntia ficus-indica* for the efficient adsorption of malachite green dye, Cu^{+2} and Ni^{+2} from water, J. Hazard. Mater., 392 (2020) 122441, doi: 10.1016/j.jhazmat.2020.122441.
[55] V.M. Muinde, J.M. Onyari, B. Wamalwa, J.N. Wabomba, Adsorption of malachite green dye from aqueous solutions using mesoporous chitosan-zinc oxide composite material, Environ. Chem. Ecotoxicol., 2 (2020) 115–125.
[56] H.A. Chanzu, J.M. Onyari, P.M. Shiundu, Brewers' spent grain in adsorption of aqueous Congo Red and malachite green dyes: batch and continuous flow systems, J. Hazard. Mater., 380 (2019) 120897, doi: 10.1016/j.jhazmat.2019.120897.
[57] M. Gao, Z. Wang, C. Yang, J. Ning, Z. Zhou, G. Li, Novel magnetic graphene oxide decorated with persimmon tannins for efficient adsorption of malachite green from aqueous solutions, Colloids Surf. A, 566 (2019) 48–57.